1. AGENCY USE ONLY (Leave blank)	2. REPORT DATE	3. REPORT TYPE AND DATES COVERED
	19 March 1993	Technical

4. TITLE AND SUBTITLE
Direct Visualization of Defect Structures Contained Within Self-Assembled Organomercaptan Monolayers: Combined Use of Electrochemistry and Scanning Tunneling Microscopy

5. FUNDING NUMBERS
N00014-91-1991

6. AUTHOR(S)
Li Sun and
Richard M. Crooks

7. PERFORMING ORGANIZATION NAME(S) AND ADDRESS(ES)
Department of Chemistry
University of New Mexico
Albuquerque, NM 87131

8. PERFORMING ORGANIZATION REPORT NUMBER
6

9. SPONSORING/MONITORING AGENCY NAME(S) AND ADDRESS(ES)
Office of Naval Research
800 North Quincy Street
Arlington, VA 22217-5000

10. SPONSORING/MONITORING AGENCY REPORT NUMBER

11. SUPPLEMENTARY NOTES
Prepared for Publication in *Langmuir*

12a. DISTRIBUTION/AVAILABILITY STATEMENT
This document has been approved for public release and sale; its distribution is unlimited

12b. DISTRIBUTION CODE
N00179

13. ABSTRACT (Maximum 200 words)

Adventitious defects within self-assembled monolayers of 1-octadecanethiol confined to Au substrate have been studied by a new method which takes advantage of the high spatial resolution of scanning tunneling microscopy (STM) and the molecular specificity of electrochemistry. The method permits direct visualization of the defect density and provides information about the chemical and structural nature of the defects. CN^- was used to electrochemically etch Au from surface regions near defects. This leads to the formation of triangular etch pits, which exhibit a uniform in-plane orientation. A point-defect model is proposed to explain the orientation of the triangular pits. The model also predicts that the organomercaptan molecules occupy particular three-fold hollow sites.

14. SUBJECT TERMS

15. NUMBER OF PAGES

16. PRICE CODE

17. SECURITY CLASSIFICATION OF REPORT	18. SECURITY CLASSIFICATION OF THIS PAGE	19. SECURITY CLASSIFICATION OF ABSTRACT	20. LIMITATION OF ABSTRACT
Unclassified	Unclassified	Unclassified	

OFFICE OF NAVAL RESEARCH

GRANT N00014-91-J-1991

R&T Code s400x084yi01

Technical Report No. 6

Direct Visualization of Defect Structures Contained Within Self-Assembled Organomercaptan Monolayers: Combined Use of Electrochemistry and Scanning Tunneling Microscopy

by

Li Sun and Richard M. Crooks

Prepared for Publication

in

Langmuir

Department of Chemistry
University of New Mexico
Albuquerque, NM 87131

March 19, 1993

[Prepared for publication as a Letter in *Langmuir*]

Direct Visualization of Defect Structures Contained Within Self-Assembled Organomercaptan Monolayers: Combined Use of Electrochemistry and Scanning Tunneling Microscopy.

Li Sun and Richard M. Crooks*

Department of Chemistry
University of New Mexico
Albuquerque, NM 87131

* Author to whom correspondence should be addressed.

Submitted: 15 March, 1993

ABSTRACT

Adventitious defects within self-assembled monolayers of 1-octadecanethiol confined to Au substrate have been studied by a new method which takes advantage of the high spatial resolution of scanning tunneling microscopy (STM) and the molecular specificity of electrochemistry. The method permits direct visualization of the defect density and provides information about the chemical and structural nature of the defects. CN^- was used to electrochemically etch Au from surface regions near defects. This leads to the formation of triangular etch pits, which exhibit a uniform in-plane orientation. A point-defect model is proposed to explain the orientation of the triangular pits. The model also predicts that the organomercaptan molecules occupy particular three-fold hollow sites.

INTRODUCTION

We report a new method for direct visualization of defect structures contained within ultrathin films, which is based on electrochemical etching and scanning tunneling microscopy (STM). Although results presented here focus exclusively on adventitious defect structures contained within 1-octadecanethiol self-assembled monolayers (SAMs) confined to Au substrates ($Au/SH(CH_2)_{17}CH_3$), the general approach should be suitable for characterizing other types of ultrathin films.[1,2] Characterization of defect sites within SAMs is particularly important, because they may play an important role in determining the average structure and chemistry of these model organic surfaces.

The approach we have taken for visualizing adventitious defect structures is illustrated in Scheme I. First, an atomically flat Au (111) surface is imaged by STM to insure uniformity. Second, the surface is modified with a monolayer of $HS(CH_2)_{17}CH_3$ that contains adventitious defects. Finally, the Au substrate is electrochemically etched in CN^-, which results in the dissolution of Au only in those regions of the organic monolayer that contain defects that have the correct chemical and structural properties to admit CN^-. There is an important distinction between the approach illustrated in Scheme I and most other electrochemical-based methods that have been used to determine the nanostructure of molecular monolayer films: previous studies have focused on determining the average properties of defects by examining the movement of electrons across the organomercaptan barrier.[3-11] However, it is nearly impossible to interpret results

obtained from experiments such as these in terms of the microscopic nature of the film, because the data are averaged over a large number of structurally and chemically distinct defects. Interpretation of data obtained only from electrochemical methods is further complicated, since electrons tunnel through thin organic layers with a facility that depends on the nature of each defect. In contrast, the combined electrochemical/STM approach reported here results in detection of individual defect sites and only those that permit complete penetration of the etchant ions to exposed regions of the Au surface. Therefore, we are able to directly visualize those regions of the monolayer that contain individual molecule-size defects that are structurally homogeneous. In this sense, our results complement previous electrochemical studies of defected monolayers,[3-11] and other techniques based on contact angle measurements[12] and temperature programmed desorption (TPD).[13]

EXPERIMENTAL

Chemicals. 1-octadecanethiol, $HS(CH_2)_{17}CH_3$, (Aldrich, 98%), KCN (Fisher), and Na_2HPO_4 (Fisher) were used as received. Water was purified (resistivity ≥ 18 MΩ-cm) by a Milli-Q reagent water system (Millipore). Other chemicals were of reagent grade purity or better.

Substrate preparation. A 0.25 mm-diameter Au wire (99.998%) was cleaned by dipping in freshly prepared "piranha solution" (3:1 concd H_2SO_4:30% H_2O_2, **Caution:** piranha solution reacts violently with organic compounds, and it should not be stored in closed

containers). Au (111) surfaces were prepared by melting the wire in a H_2/O_2 flame under a N_2 blanket and then annealing in a cooler region of the flame.[14-16] This treatment results in approximately 0.6 mm-diameter spheres that contain a few Au (111) facets on the surface. The single-grain facets are typically elliptical with a long axis of about 100 μm, and they are composed of atomically flat terraces that are usually at least 100 nm wide. Immediately prior to monolayer adsorption, the Au spheres were electrochemically annealed in an aqueous 0.1 M $HClO_4/5x10^{-5}$ M HCl solution: this process desorbs organic material from the Au surface and tends to reduce the number of Au surface defects (Figure 1).[15,17] The Au spheres were modified by immersing in a 0.5 mM ethanolic solution of $HS(CH_2)_{17}CH_3$.

Electrochemistry. Electrochemical experiments were performed in a single-compartment, three-electrode, glass cell containing a Ag/AgCl, NaCl(3 M) reference electrode and a Pt counter electrode. Oxygen was not removed from the electrolyte solution prior to CN^- etching.

STM analysis. A NanoScope III scanning tunneling microscope (Digital Instruments, Santa Barbara, CA) was used for all STM experiments. Images were obtained using a bias voltage of +300 mV and tip currents in the range of 0.15 to 0.30 nA (scan rate = 2.00 Hz). Positive bias voltages indicate that electrons tunnel from the STM tip to the Au substrate. Tips were mechanically cut from Pt/Ir (80/20) wire. The STM *z*-piezo was calibrated by measuring several independently prepared Au (111) monoatomic step edges and

correlating the mean experimental value to the theoretical Au (111) interlayer spacing of 0.235 nm.[18,19]

RESULTS AND DISCUSSION

We modified a freshly prepared Au (111) surface by immersing it in a dilute ethanol solution of $HS(CH_2)_{17}CH_3$ for 1 min, and then rinsing it with ethanol and water. Previously, we found that this brief deposition treatment results in many apparent defect sites.[15] Next, we etched the SAM-modified substrate electrochemically for 30 s at a constant potential of +0.1 V in an air-saturated aqueous electrolyte solution containing 0.1 M KCN and 0.1 M Na_2HPO_4. This step results in the dissolution of Au in the form of $Au(CN)_2^-$.[20] After rinsing with water and drying under flowing N_2, we mounted the etched surface on a home-built substrate holder and obtained STM images.

In contrast to the naked Au surface shown in Figure 1, the STM image of the CN^--etched, SAM-modified Au surface (Figures 2 and 3) indicates several distinctive features. First, CN^- etching of the modified Au (111) surface results in triangular pits that are highly anisotropic: the pit widths are much larger than their depths. The triangles expand in the surface plane in direct proportion to the amount of Faradaic charge passed during the electrochemical etching step and, as shown in Figure 2, they are nearly equilateral. The three-fold symmetry of the etch pits, in conjunction with previously reported X-ray and reflection electron microscopy studies,[14,21,22] confirms our assumption that the surface possesses (111) orientation. The depths of the triangular pits

shown in Figure 2 are 0.59±0.07 nm, or about 2.5±0.3 times the theoretical interlayer spacing of Au (111), d_{Au} = 0.235 nm. In at least one case (Figure 3), the bottom of the pit can be resolved into two levels: the depth of the first level is about 1.5 d_{Au}, while the depth of the second level is about 2.5 d_{Au}. The second curious aspect of Figure 2 concerns the orientation of the triangular pits: they all point in the same direction relative to an edge of the STM image.[23] In addition, the centers of the etch pits tend to be located on step edges that were present prior to electrochemical etching (Figures 2 and 3). Finally, small round pits, 2-5 nm in diameter (Figure 3), which are absent on the naked Au surface (Figure 1), are present before and after CN^- etching. These small pits are formed during the self-assembly process, but the presence of only a few triangles indicates that they do not permit penetration by CN^-.

We do not fully understand why the triangular pits etch anisotropically. Under identical etching conditions, STM images indicate that nominally naked Au (111) surfaces etch isotropically to yield very rough surfaces, which do not exhibit the well-defined, isolated triangles shown in Figures 2 and 3. McCarley and Bard have also noted roughening of Au (111) surfaces that were chemically etched in air-saturated 0.01 M CN^- solutions.[24] There are two apparent explanations for the observation of anisotropic etching. First, it is possible that the surface or the bottom of the etch pits are protected by surface-confined organomercaptans throughout the etching process. Second, the size of the pits may be so small that etching proceeds along a completely different

pathway than it does for macroscopic naked Au surfaces. We tend to favor the latter explanation.

Figure 3 suggests that up to two atomic layers of Au are removed to form the etch pits, but the uncertainty in the chemical composition of the bottoms of the pits complicates a definitive interpretation of the actual depth. Since the height difference in the *z*-direction (Δz_2 in Scheme I) between unetched Au and the first layer of etched Au is about 1.5 d_{Au}, the extra factor of 0.5, about 0.12 nm, must be due to a difference in the tunneling probability between organomercaptan-covered Au and the etched Au (Δz_1 in Scheme I). This value is different than that observed by Kim and Bard: they reported that the difference in tunneling probability between a $HS(CH_2)_{17}CH_3$-covered Au surface and bare Au surfaces causes an apparent height difference of 0.8 nm.[25] It is difficult to reconcile this apparent discrepancy because of the uncertainty in the chemical composition of the bottom of the pits in both our experiments and in those reported by Kim and Bard. For example, we can be certain that at least one atomic layer of Au is removed to form the bottom of the first terrace, but the bottom could be covered with a monolayer or submonolayer of the organomercaptan or CN^-. The pits described by Kim and Bard might also be at least partially accounted for by removal of Au atoms from the substrate surface.[25]

We now turn our attention to the uniform in-plane orientation of the pits. There are two models that can account for this behavior. In the first model, crystal dislocations present on the Au (111) surface code for imperfections or defects witnin the

organomercaptan monolayer. At such defect sites, CN^- may readily penetrate the monolayer and facilitate Au etching. The main evidence for this model comes from several older studies of dislocation etch pits on bare (111) surfaces of fcc metals, which showed that all the etch pits exhibit uniform in-plane orientation.[26-28] Unfortunately, the mechanism for the formation of the dislocation etch pits has not been discussed, and a direct correlation between the presence of the etch pits and surface dislocations has not been proven.[26-28] Moreover, we did not detect any obvious dislocations on the Au surfaces before or after monolayer modification. McCarley and Bard have recently shown that even screw dislocations do not appear to etch at higher rates than non-defected regions of the surface under conditions similar to those we used.[24] Direct evidence for other types of dislocations, especially those having their Burgers vectors parallel to Au surfaces,[29] may only be attainable from *in-situ* and atomically resolved STM measurements. Since this dislocation model does not explicitly account for the anisotropic structure or the in-plane orientation of the CN^- etch pits, we propose an alternative, namely, the point-defect model.

A single closed-packed Au (111) plane, denoted as plane A in Scheme II, possesses six-fold symmetry. This symmetry, however, is reduced to three-fold symmetry when a second (111) plane, plane B, is placed below plane A. The presence of plane B results in two structurally and chemically distinct three-fold hollow sites in plane A: one has an Au atom directly below it, while the other has an octahedral interstice below it. Adsorption of an

organomercaptan on either site will conserve and reinforce three-fold symmetry. The $(\sqrt{3} \times \sqrt{3})R30°$ lattice of the adsorbed organic monolayer[2,30-34] requires that all organomercaptans occupy identical three-fold hollow sites. Therefore, all triangles formed by the three Au atoms that define a particular type of three-fold hollow site will possess the same in-plane orientation (Scheme II). We propose that point defects, which are created within the framework of the organomercaptan monolayer by the absence of one molecule from a three-fold hollow site (Scheme II, sites *a* and *b*), act as nucleation sites for CN^- etching. That is, each defect site reveals 3 equivalent Au atoms that are exposed to attack from CN^-. Following dissolution of the first 3 Au atoms, 3 additional organomercaptans desorb prior to removal of 12 additional Au atoms (Scheme II, site b). Continuation of this process will result in triangular etch pits, such as those observed in Figure 2, which all point in the same direction. Moreover, this point-defect model predicts that the orientation of the triangles will be the same regardless of the terrace on which they reside (Scheme II). As shown in Figure 2, we also observe this behavior experimentally. Step edges do not influence the in-plane orientation of the etched pits, but they do play an important role in the initial formation of the monolayer defects, as evidenced by the location of the etch pits (Figure 2).

The results presented in Figure 2 lead to another interesting conclusion. Thus far we have assumed that adsorbed organomercaptans occupy three-fold hollow sites on the Au (111) lattice, but the $(\sqrt{3} \times \sqrt{3})R30°$ lattice of the thiol monolayer does

not preclude adsorption at the six-fold on-top sites. In this case, a point defect, formed by removing one adsorbate molecule from an on-top site, will expose 6 equivalent Au atoms that are subject to attack by CN^-. Sequential etching will result in formation of two sets of triangular etch pits with one set rotated 60° relative to the other. Since this behavior is not observed experimentally, we conclude that the three-fold hollow sites are preferred by surface-confined thiol molecules. Although we are not able to assign the type of three-fold follow sites occupied by the organomercaptan, this result is significant since previous studies have only established the $(\sqrt{3}x\sqrt{3})R30°$ lattice; not the nature or type of the adsorption sites.[2,30-34]

In addition to revealing a chemically homogeneous set of individual defect sites, our results also clarify the chemical nature of the small round features, which appear as 2-5 nm-diameter pits in Figure 3. It is obvious that these pits are not electrochemically active under the etching conditions used in this work. Therefore, we do not believe they represent depressions in the organic adlattice. Instead, our results are consistent with two recent reports that indicate that organomercaptans dissolve Au.[35,36] We believe the defects are present in the Au lattice rather than in the organic adlattice. If the pits were anything other than craters in the Au surface, they would be large enough to permit entry by CN^- and would result in formation of etch pits.

CONCLUSIONS

We have described a new method for studying defects contained within self-assembled organomercaptan monolayers confined to Au substrates, which takes advantage of the high spatial resolution of scanning tunneling microscopy (STM) and the molecular specificity of electrochemistry. The method permits direct counting of defect sites and also provides some clarification of the chemical and the structural nature of the defects.

The results presented here will be of benefit to several related areas of research. First, our method permits direct measurement of the nearest-neighbor defect distance. Indirect electrochemical methods for determining defect densities[37] require knowledge of this variable, but it has thus far been elusive.[5a,7,38] Second, it is critical to know the defect density and the effects of defects when self-assembled monolayers are used for modeling electron transfer processes. Our method should prove beneficial to those studies, which heretofore have relied on assumptions and indirect measurements of defect densities.[5b,6b,10,11] Third, one aspect of our current research focuses on the synthesis of defects with controlled sizes and shapes. Recently, we have probed these intentionally created defects using electrochemical techniques.[38] The method presented here will permit us to obtain more direct information concerning the nature and spatial distribution of these intentionally formed defect structures.

ACKNOWLEDGMENT

Full support of this research by the Office of Naval Research is gratefully acknowledged. We also acknowledge a very helpful discussion with Professor Robert M. Corn (University of Wisconsin, Madison).

REFERENCES

1. Nuzzo, R. G.; Allara, D. L. *J. Am. Chem. Soc.* **1983**, *105*, 4481.
2. Dubois, L. H.; Nuzzo, R. G. *Annu. Rev. Phys. Chem.* **1992**, *43*, 437, and references therein.
3. (a) Sabatani, E.; Rubinstein, I.; Maoz, R.; Sagiv, J. *J. Electroanal. Chem.* **1987**, *219*, 365. (b) Rubinstein, I.; Steinberg, S.; Tor, Y.; Shanzer, A.; Sagiv, J. *Nature* **1988**, *332*, 426.
4. Porter, M. D.; Bright, T. B.; Allara, D. L.; Chidsey, C. E. D. *J. Am. Chem. Soc.* **1987**, *109*, 3559.
5. (a) Finklea, H. O.; Snider, D. A.; Fedyk, J. *Langmuir* **1990**, *6*, 371. (b) Finklea, H. O.; Hanshew, D. D. *J. Am. Chem. Soc.* **1992**, *114*, 3173.
6. (a) Chidsey, C. E. D.; Loiacono, D. N. *Langmuir* **1990**, *6*, 682. (b) Chidsey, C. E. D.; Bertozzi, C. R.; Putvinski, T. M.; Mujsce, A. M. *J. Am. Chem. Soc.* **1990**, *112*, 4301.
7. (a) Bilewicz, R.; Majda, M. *J. Am. Chem. Soc.* **1991**, *113*, 5464. (b) Bilewicz, R.; Majda, M. *Langmuir* **1991**, *7*, 2794.
8. Collard, D.; Fox, M. A. *Langmuir* **1991**, *7*, 1192.
9. Creager, S. E.; Hockett, L. A.; Rowe, G. K. *Langmuir* **1992**, *8*, 854.
10 Hong, H.-G.; Mallouk, T. E. *Langmuir* **1991**, *7*, 2362.
11. Miller, C.; Cuendet, P.; Gratzel, M. *J. Phys. Chem.* **1991**, *95*, 877.

12. (a) Bain, C. D.; Troughton, E. B.; Tao, Y.-T.; Evall, J.; Whitesides, G. M.; Nuzzo, R. G. *J. Am. Chem. Soc.* **1989**, *111*, 321. (b) Bain, C. D.; Whitesides, G. M. *J. Am. Chem. Soc.* **1988**, *110*, 5859.

13. (a) Dubois, L. H.; Zegarski, B. R.; Nuzzo, R. G. *Proc. Natl. Acad. Sci. USA* **1987**, *84*, 4739. (b) Dubois, L. H.; Zegarski, B. R.; Nuzzo, R. G. *J. Am. Chem. Soc.* **1990**, *112*, 570.

14. Hsu, T. *Ultramicroscopy* **1983**, *11*, 167.

15. Sun, L.; Crooks, R. M. *J. Electrochem. Soc.* **1991**, *138*, L23.

16. Snyder, S. R. *J. Electrochem. Soc.* **1992**, *139*, 5C.

17. Trevor, D. J.; Chidsey, C. E. D.; Loiacono, D. N. *Phys. Rev. Lett.* **1989**, *62*, 929.

18. The interlayer spacing of Au (111) planes was calculated from the nearest neighbor spacing, 0.2884 nm (*CRC Handbook of Chemistry and Physics, 61st ed.*; Weast, R. C., Ed.; CRC Press: Boca Raton, FL, 1980; p F-219).

19. To accurately measure the step height, an appropriate portion of an STM image was first processed using the "manual flatten" feature of the NanoScope III software, then the histogram of all the pixel values within the selected portion was analyzed. Pixels on the same atomically-flat terrace correspond to a peak in the histogram. By measuring the distance between two well-resolved histogram peaks, the step height can be determined with better reliability than that determined by measuring two arbitrary points on each terrace. The full width at half

maximum of a histogram peak was used as the uncertainty of the height measurements.

20. (a) Milazzo, G. *Electrochemistry*; Elsevier: Amsterdam, 1963; p 161. (b) Kirk, D. W.; Foulkes, F. R. *J. Electrochem. Soc.* **1980**, *127*, 1993.

21. Clavilier, J.; Faure, R.; Guinet, G.; Durand, R. *J. Electroanal. Chem.* **1980**, *107*, 205.

22. Hsu, T.; Cowley, J. M. *Ultramicroscopy* **1983**, *11*, 239.

23. We appreciate Professors Michael D. Ward and Henry S. White (University of Minnesota) pointing this out to us.

24. McCarley, R. L.; Bard, A. J. *J. Phys. Chem.* **1992**, *96*, 7410.

25. Kim, Y.-T.; Bard, A. J. *Langmuir* **1992**, *8*, 1096.

26. Chen, C. C.; Hendrickson, A. A. *J. Appl. Phys.* **1971**, *42*, 2208.

27. Basinski, Z. S.; Basinski, S. J. *Phil. Mag.* **1964**, *9*, 51.

28. Hashimoto, S.; Miura, S.; Kubo, T. *J. Mater. Sci.* **1976**, *11*, 1501.

29. Friedel, J. *Dislocations*; Addison-Wesley: Reading, PA, 1967; Chapter 1.

30. Strong, L.; Whitesides, G. M. *Langmuir* **1988**, *4*, 546.

31. Chidsey, C. E. D.; Liu, G.; Rowntree, P.; Scoles, G. *J. Chem. Phys.* **1989**, *91*, 4421.

32. (a) Samant, M. G.; Brown, C. A.; Gordon, J. G., II *Langmuir* **1992**, 7, 437. (b) Samant, M. G.; Brown, C. A.; Gordon, J. G., II *Langmuir* **1992**, *8*, 1615.

33. Kim, Y.-T.; McCarley, R. L.; Bard, A. J. *J. Phys. Chem.* **1992**, *96*, 7416.

34. Widrig, C. A.; Alves, C. A.; Porter, M. D. *J. Am. Chem. Soc.* **1991**, *113*, 2805.

35. McCarley, R. L.; Kim, Y.-T.; Bard, A. J. *J. Phys. Chem.* **1993**, *97*, 211.

36. Edinger, K.; Golzhauser, A.; Demota, K.; Woll, C.; Grunze, M. *Langmuir* **1993**, *9*, 4.

37. Amatore, C.; Savéant, J. M.; Tessier, D. *J. Electroanal. Chem.* **1983**, *147*, 39.

38. Chailapakul, O.; Crooks, R. M. *Langmuir*, in press.

FIGURE CAPTIONS

Figure 1. STM image of an atomically-flat Au (111) facet on a flame- and electrochemically-annealed Au sphere.

Figure 2. STM images of a CN^--etched, $HS(CH_2)_{15}CH_3$-modified Au (111) surface. The scan area is 1000 nm by 1000 nm. The sides of the equilateral triangular etch pits are 65 ± 8 nm.

Figure 3. A close-up image of the triangular etch-pit located near the center of Figure 2. The scan area is 200 nm by 200 nm.

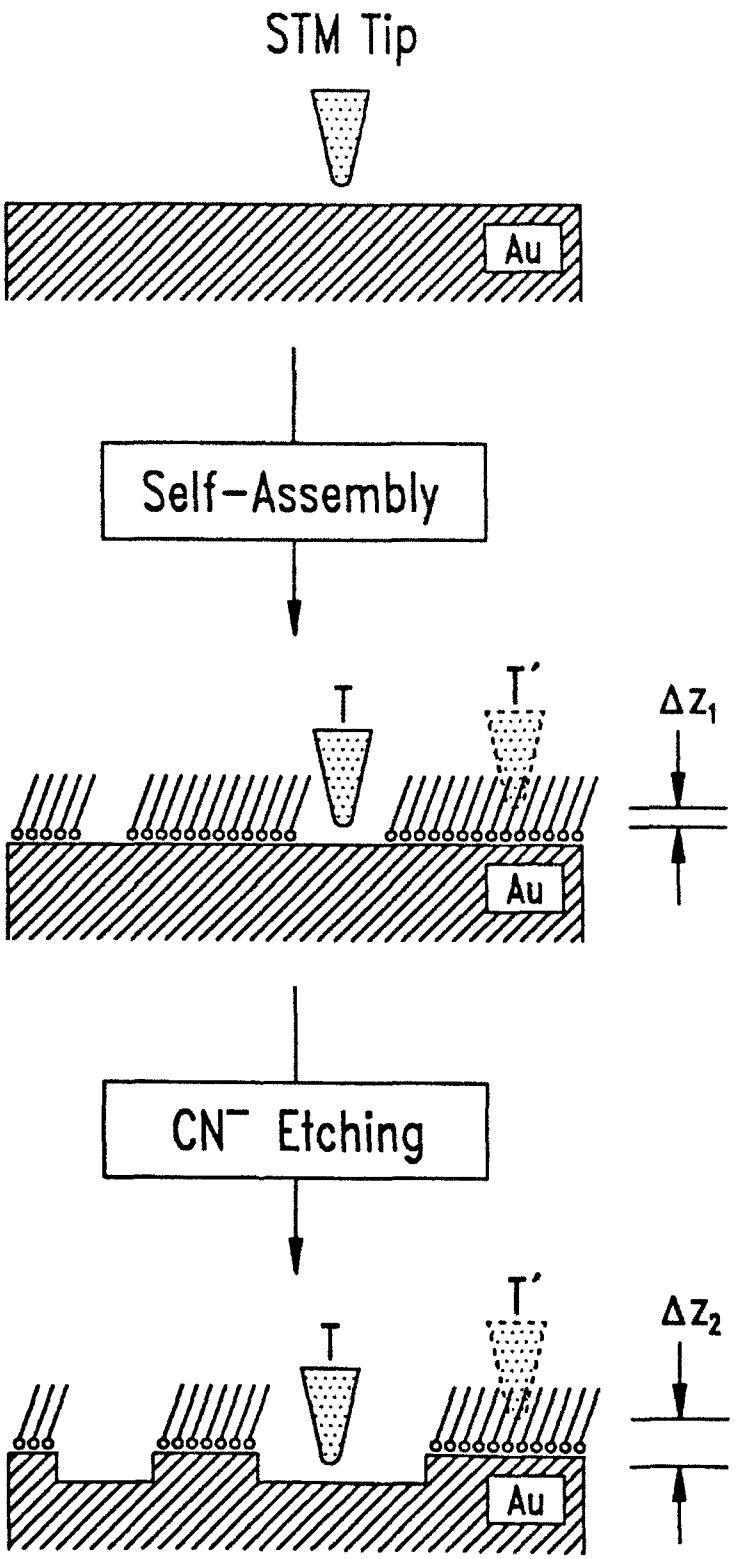

Scheme I /Sun et al.

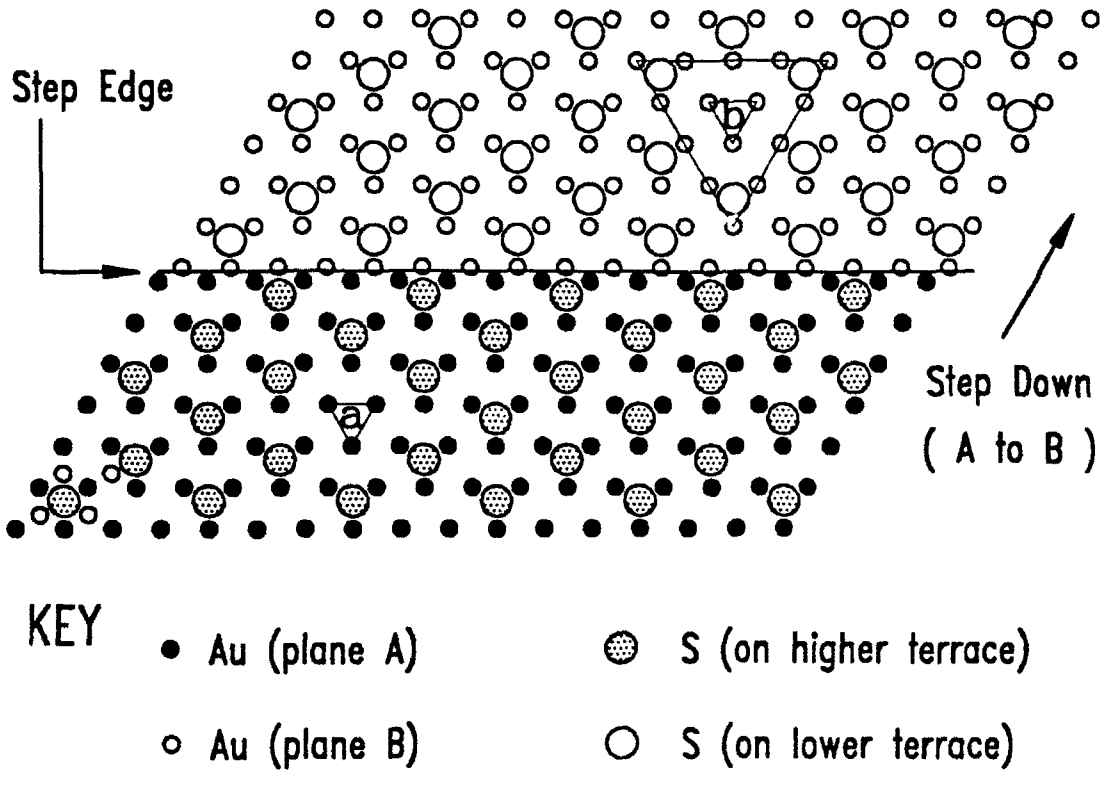

Scheme II /Sun et al.

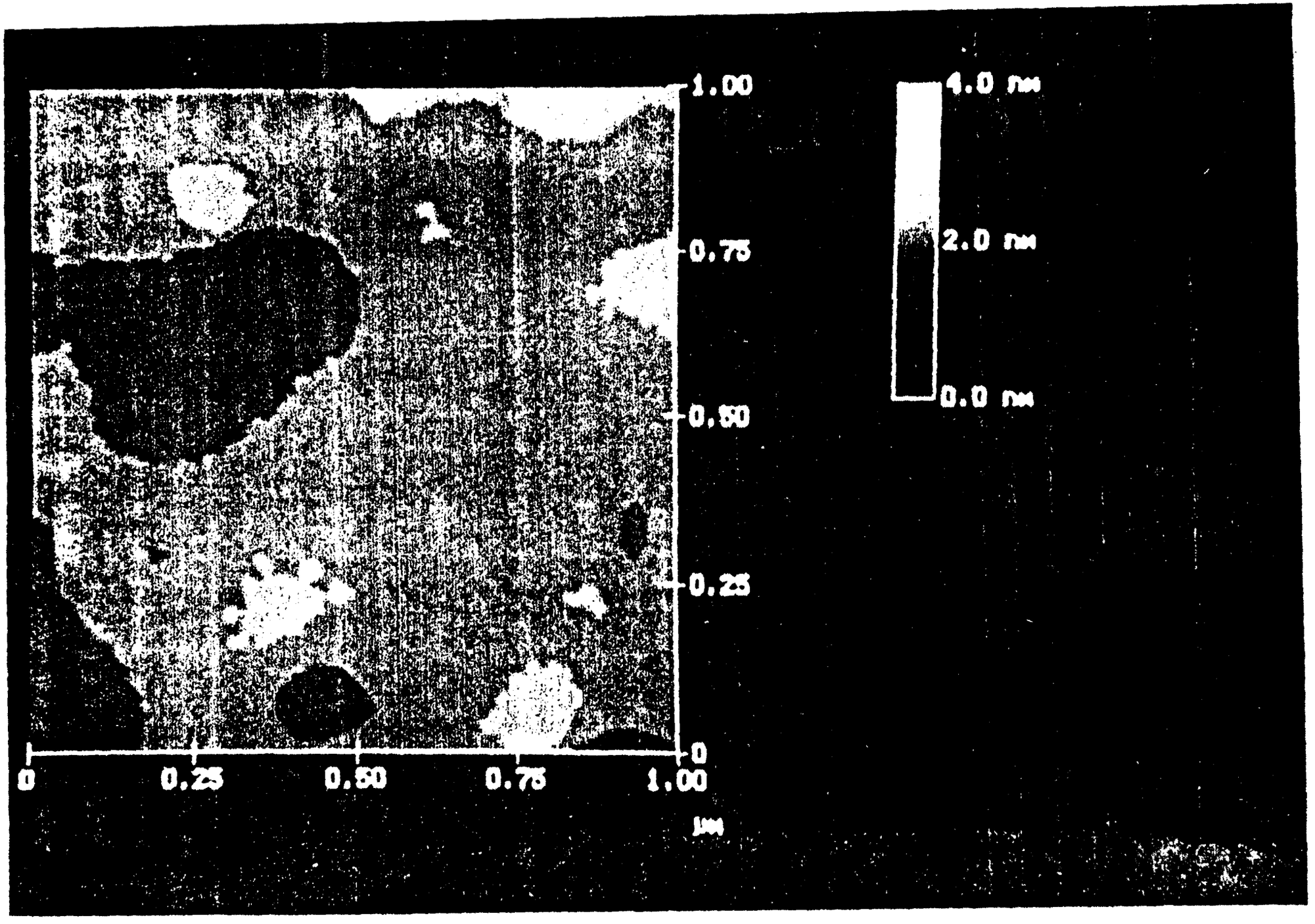

Figure 1, Sun et al.

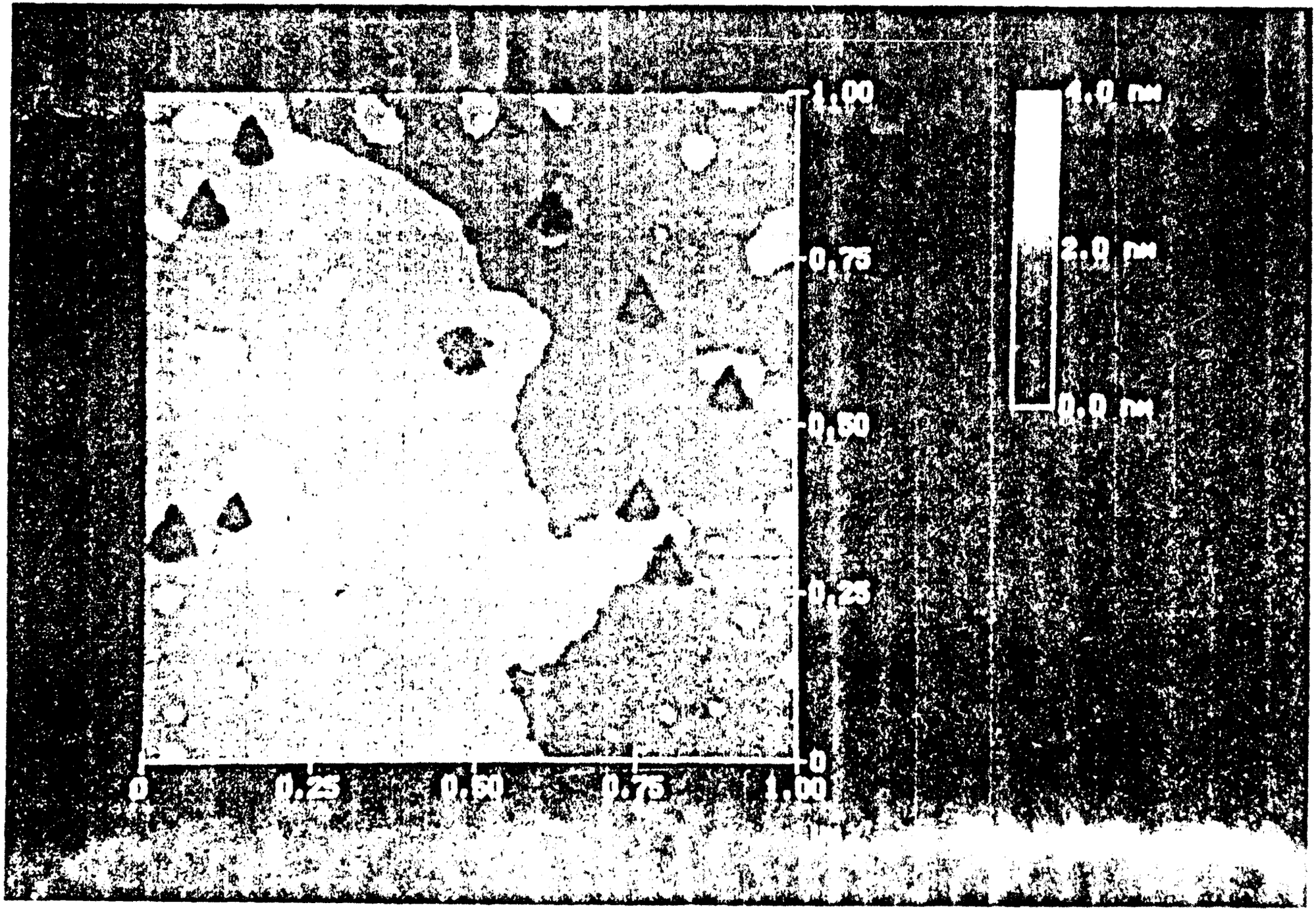
1,00
0,75
0,50
0,25
0
0
0,25
0,50
0,75
1,00
1,0 nm
0,5 nm
0,0 nm

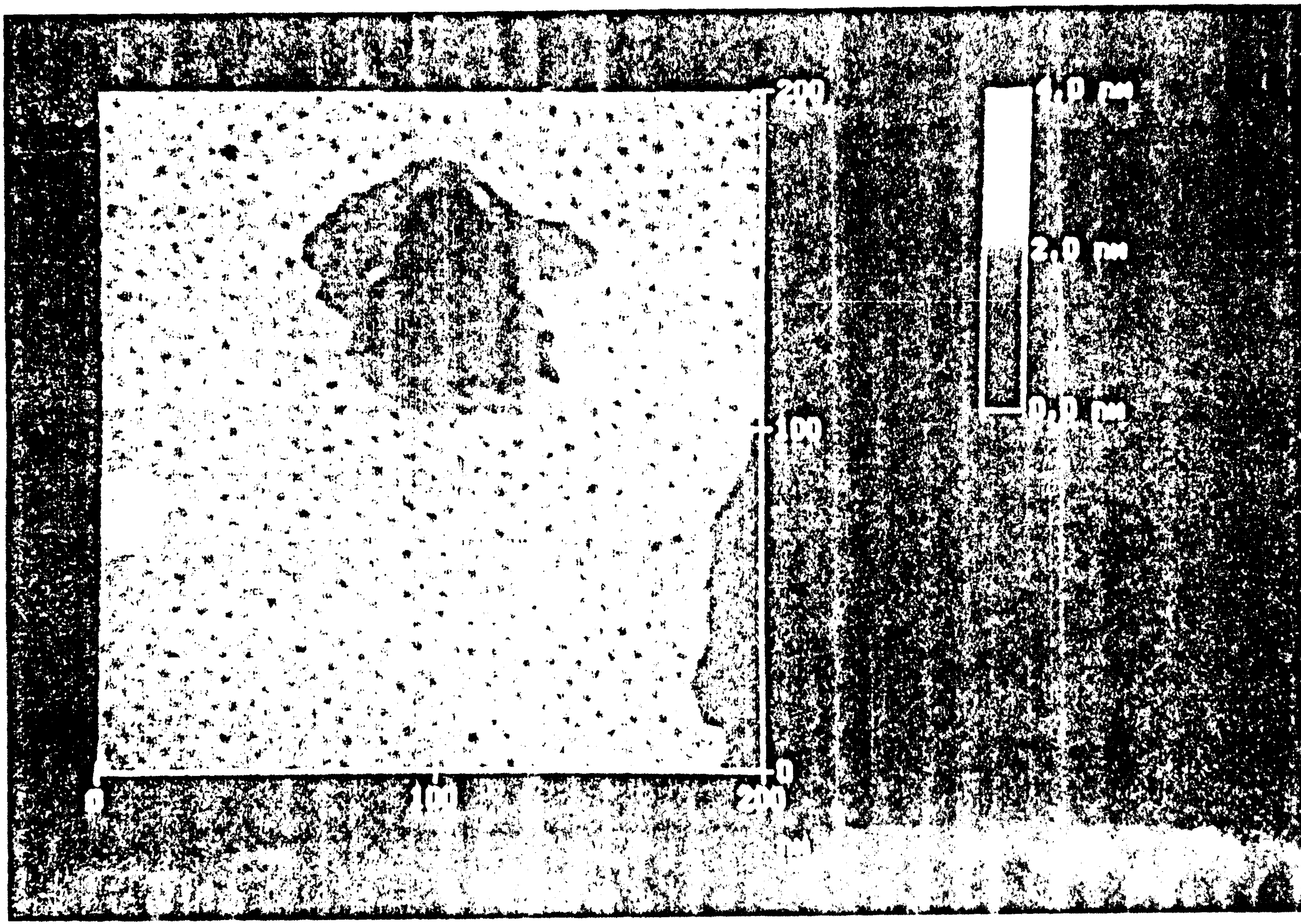
4.0 nm
2.0 nm
0.0 nm
200
100
0
0
100
200

TECHNICAL REPORT DISTRIBUTION LIST - GENERAL

Office of Naval Research (2)*
Chemistry Division, Code 1113
800 North Quincy Street
Arlington, Virginia 22217-5000

Dr. James S. Murday (1)
Chemistry Division, Code 6100
Naval Research Laboratory
Washington, D.C. 20375-5000

Dr. Robert Green, Director (1)
Chemistry Division, Code 385
Naval Air Weapons Center
Weapons Division
China Lake, CA 93555-6001

Dr. Elek Lindner (1)
Naval Command, Control and Ocean
Surveillance Center
RDT&E Division
San Diego, CA 92152-5000

Dr. Bernard E. Douda (1)
Crane Division
Naval Surface Warfare Center
Crane, Indiana 47522-5000

Dr. Richard W. Drisko (1)
Naval Civil Engineering
Laboratory
Code L52
Port Hueneme, CA 93043

Dr. Harold H. Singerman (1)
Naval Surface Warfare Center
Carderock Division Detachment
Annapolis, MD 21402-1198

Dr. Eugene C. Fischer (1)
Code 2840
Naval Surface Warfare Center
Carderock Division Detachment
Annapolis, MD 21402-1198

Defense Technical Information
Center (2)
Building 5, Cameron Station
Alexandria, VA 22314

* Number of copies to forward